

Supporting Information

**Insights into Zn Anode Surface Chemistry for Dendrite-Free Zn Ion Batteries**

Qiang Hu<sup>a,+</sup>, Jisong Hu<sup>c,+</sup>, Yuanxia Li<sup>a</sup>, Xinyi Zhou<sup>a</sup>, Shixiang Ding<sup>a</sup>, Qiaoji Zheng<sup>a,\*</sup>,  
Dunmin Lin<sup>a</sup>, Jingxin Zhao<sup>b,\*</sup>, Bingang Xu<sup>b,\*</sup>

*a. College of Chemistry and Materials Science, Sichuan Normal University, Chengdu  
610066, China*

*b. Nanotechnology Center, Institute of Textiles and Clothing, The Hong Kong  
Polytechnic University, Hung Hom, Kowloon, Hong Kong, 999077, P. R. China*

*c. School of Optical and Electronic Information, Huazhong University of Science and  
Technology, Wuhan 430074, China*

E-mail: [\*] joyce@sicnu.edu.cn (Qiaoji Zheng); jingxzhao@polyu.edu.hk (Jingxin  
Zhao); tcxubg@polyu.edu.hk (Bingang Xu)

[+] These authors contribute equally to this work

# Table of Contents for Supplemental Information

## 1. Supplemental Experimental Details

### 2. Supporting Notes

2.1 The strategy for using of TS electrolyte additives and establishment of a dense ZnO@Cu artificial layer on the surface of Zn metal for constructing dendrite-free Zn electrode without side reaction.

2.2 The study of CE.

2.3 The study of deposition orientation of Zn<sup>2+</sup> using TS additive.

2.4 Structural characterization (SEM, XRD and BET) of the NH<sub>4</sub>V<sub>3</sub>O<sub>8</sub> electrode materials.

2.5 Galvanostatic cycling of the NH<sub>4</sub>V<sub>3</sub>O<sub>8</sub>|ZnO@Cu/Zn-TS cell and co-intercalation mechanism of Zn<sup>2+</sup> and NH<sub>4</sub><sup>+</sup>.

### 3. Supporting Figures

**Fig. S1.** SEM images of bare Zn foil.

**Fig. S2.** SEM images of the Zn foil in 2 M ZnSO<sub>4</sub> after 5 days.

**Fig. S3.** SEM image of Zn foil in 2 M ZnSO<sub>4</sub> with TS after 5 days.

**Fig. S4.** Electrochemical impedance spectroscopy measurements of various Zn cells.

**Fig. S5.** a) Introducing the ZnO@Cu layer on the surface of Zn metal substrate by two-step strategy. b) By incorporating the artificial ZnO@Cu layer on the Zn surface and using TS electrolyte additive, uniform and compact Zn plating behavior without side reactions can be obtained.

**Fig. S6.** SEM image of the ZnO@Cu/Zn in 2 M ZnSO<sub>4</sub> after 5 days.

**Fig. S7.** XRD patterns of ZnO@Cu/Zn foil before and after the soaking in 2 M ZnSO<sub>4</sub> for 5 days.

**Fig. S8.** X-ray diffraction (XRD) patterns of Cu on Carbon cloth.

**Fig. S9.** EDS mapping images of ZnO@Cu/Zn including Zn, Cu and O element.

**Fig. S10.** SEM, TEM and HR-TEM images of ZnO@Cu/Zn.

**Fig. S11.** Transmission mapping images of ZnO@Cu/Zn including Zn, Cu and O element.

**Fig. S12.** High-resolution XPS spectra of Cu in ZnO/Zn and ZnO@Cu/Zn.

**Fig. S13.** Model of DFT calculations, showing a hydrated Zn<sup>2+</sup> ion passing on a Zn surface.

**Fig. S14.** Linear polarization curves showing the corrosion on bare Zn, Zn-TS, ZnO@Cu/Zn and ZnO@Cu/Zn-TS.

**Fig. S15.** (a) Nyquist plots collected at open circuit voltage (OCV) over the frequency range of 100 kHz to 1 Hz. a) Zn symmetrical cell with glass fibre as separator (inset: enlargement of indicated range). b) ZnO@Cu coated Zn symmetrical cell with glass fibre as separator (inset: enlargement of indicated range).

**Fig. S16.** Comparison of HER performance under Zn and ZnO@Cu/Zn-TS electrodes systems.

**Fig. S17.** a) Zn-TS and b) ZnO@Cu/Zn electrodes in symmetric transparent cells, along with the specified numbers of plating/stripping cycles.

**Fig. S18.** Coulombic efficiency (CE) measurements of Zn//Ti and Zn//ZnO@Cu/Ti-TS cells under different electrolyte system and b) corresponding voltage profiles at

various cycles.

**Fig. S19.** a) Comparison of the cycling stability of Zn, Zn-TS, ZnO@Cu/Zn and ZnO@Cu/Zn-TS symmetric cell at  $0.5 \text{ mA cm}^{-2}$  with the capacity of  $2 \text{ mA h cm}^{-2}$ ; b) High-resolution voltage profiles at  $0.5 \text{ mA cm}^{-2}$  with the capacity of  $2 \text{ mA h cm}^{-2}$  for the first cycle.

**Fig. S20.** Top-view SEM images of Zn deposition for ZnO@Cu/Zn-TS electrodes after a) 100 cycles, b) 200 cycles and c) 400 cycles; d) Cross-sectional SEM image of Zn deposition for ZnO@Cu/Zn-TS electrodes after 400 cycles at  $10 \text{ mA cm}^{-2}$  and  $2 \text{ mA cm}^{-2}$ .

**Fig. S21.** Cross-sectional mapping images of ZnO@Cu/Zn including Zn, Cu and O element of Zn deposition for ZnO@Cu/Zn-TS electrodes after 400 cycles at  $10 \text{ mA cm}^{-2}$  and  $2 \text{ mA cm}^{-2}$ .

**Fig. S22.** XRD pattern of  $\text{NH}_4\text{V}_3\text{O}_8$ .

**Fig. S23.** SEM images of  $\text{NH}_4\text{V}_3\text{O}_8$ .

**Fig. S24.** Pore size distribution curves of  $\text{NH}_4\text{V}_3\text{O}_8$ .

**Fig. S25.** Rate performance based on charging/discharging curves of the  $\text{NH}_4\text{V}_3\text{O}_8|\text{Zn}$ ,  $\text{NH}_4\text{V}_3\text{O}_8|\text{Zn-TS}$ ,  $\text{NH}_4\text{V}_3\text{O}_8|\text{ZnO@Cu/Zn}$  and  $\text{NH}_4\text{V}_3\text{O}_8|\text{ZnO@Cu/Zn-TS}$  battery.

**Table S1.** Comparison of the adsorption energy of  $\text{Zn}^{2+}$  ions of Zn, ZnO and Cu at bridge, top and hole view.

**Table S2.** The calculated lattice constants and corresponding k-point mesh of the bulk and surface structures.

**Table S3.** Results of electrical conductivity measurement performed on Zn foil,

ZnO@Cu/Zn and ZnO@Cu powder.

**Table S4.** Comparison of the electrolyte additives or artificial layer of symmetric cells for Zn dendrite inhibition.

## 1. Supplemental Experimental Details

**1.1 Materials.** Zn foil (~0.1 mm) and Pt were purchased from Haoxuan Metal Material Co., Ltd. ZnSO<sub>4</sub>·7H<sub>2</sub>O (>99.0%), CuSO<sub>4</sub>·5H<sub>2</sub>O (>99.0%), tetramethylammonium sulfate (TS, >99.98%), Ag/AgCl electrode, Ammonium persulfate (APS, >99.99%) and V<sub>2</sub>O<sub>5</sub> powder (>99.99%) were purchased from Sinopharm Chemical ReagentCo., Ltd. All other reagents were analytical grade and used directly without further purification. Deionized water was used to prepare all aqueous electrolytes.

### 1.2 Materials Preparation:

Synthesis of ZnO@Cu/Zn: The commercial Zn foil was cut into Zn ribbons (2 cm × 6 cm), and then one side of the Zn ribbon was carefully polished with sandpaper to remove the passivation layer. A polished Zn ribbons were put into a specially designed tube. The product was rinsed by distilled water and ethanol several times and subsequently calcined at 350 °C for 6 h at a ramp rate of 5 °C min<sup>-1</sup> under air atmosphere. Prior to the electrodeposition, the treated Zn foil was immersed into 100 mL of a solution containing CuSO<sub>4</sub>·5H<sub>2</sub>O (0.1 M) with an immersed area of 2 cm × 3 cm. During the electrodeposition using an electrochemical workstation (CHI760E, Shanghai, China), the treated Zn foil was used as the working electrode, while platinum (Pt) wire and Ag/AgCl were used as a counter electrode and a reference

electrode, respectively. The deposition was performed for 1,000 s under the static potential of -1.5 V (vs. Ag/AgCl). The material was taken out and rinsed with deionized water and ethanol several times. The resulting Zn foil was dried at 60 °C for 12 h in a vacuum oven.

Synthesis of  $\text{NH}_4\text{V}_3\text{O}_8$ : 0.4 g  $\text{V}_2\text{O}_5$  and 0.2 g APS were dissolved in 50 ml of deionized water under magnetic stirring to form solution. The reaction solution was subsequently transferred into a 100 mL Teflon-lined stainless-steel autoclave and kept at 95 °C for 48 h. After cooled to room temperature, the powder was cleaned with deionized water and ethanol several times.

### **1.3 Materials Characterization:**

The micromorphology of the samples was observed using scanning electron microscopy (SEM, FEI-Quanta 250, USA). The elemental analysis of the samples was characterized using a scanning electron microscope (FE-SEM, JSM-7500, Japan) equipped with corresponding energy-dispersive X-ray (EDX) elemental mapping. The crystal structure of the samples was characterized through the X-ray diffraction analysis (XRD, Smart Lab, Rigaku, Japan) with Cu-K $\alpha$  ( $\lambda = 1.540598 \text{ \AA}$ , Smart Lab) source (scan rate of  $2 \text{ }^\circ\text{min}^{-1}$ ) in the  $2\theta$  range of  $10^\circ \sim 80^\circ$ . The surface element analysis of the samples was carried out by a PHI 5000 VersaProbe XPS instrument (XPS, Thermo ESCALAB 250XI, USA) and Fourier transform infrared spectrum (FTIR, NICOLET iS50, USA).

### **1.4 Electrochemical Tests:**

Electrochemical characterization of symmetrical Zn, Zn-TS, ZnO@Cu/Zn and

ZnO@Cu/Zn-TS cells was conducted using both transparent cells and 2032-type coin-cells. Electrochemical impedance spectroscopy (EIS) of these cells were conducted on an electrochemical workstation (CHI660E, Shanghai, China) over the frequency range of 100 kHz to 1 Hz. The cells were galvanostatically charged/discharged in the voltage range of 0.4 – 1.6 V vs. Zn/Zn<sup>2+</sup> at different current densities on a Land CT5001A battery tester, and the specific capacities were calculated based on the active mass of NH<sub>4</sub>V<sub>3</sub>O<sub>8</sub> cathode. The mass of active material was ~1.1 mg.

### ***1.5 Transparent Zn Cell and In Situ Dendrite Observation:***

A transparent Zn-Zn cell was designed to observe the Zn dendrite growth. Specifically, a transparent glass dish, two Zn ribbons (0.5 cm × 3 cm), and two plastic clamps form a pool for observing the Zn dendrites. The transparent glass dish is used to store the electrolyte. The Zn dendrites growth was in situ observed by an optical microscope equipped with a digital camera. Meanwhile the transparent Zn cell was tested for Zn stripping/plating using an electrochemical workstation (CHI660E).

### ***1.6 Theoretical Calculations:***

All calculations were carried out with the Vienna ab initio simulation package (VASP).<sup>1</sup> The electronic exchange-correlation energy was implemented using the Perdew-Burke-Ernzerhof (PBE) functional within the generalized gradient approximation (GGA).<sup>2</sup> A cutoff energy of 500 eV for plane-wave basis set was adopted. As for geometric optimization, the atomic positions were optimized until all components of the forces on each atom were less than -0.05 eV/Å and the total energy converge was set to below 10<sup>-4</sup> eV. The DFT-D3 correction was used to describe van

der Waals interactions.<sup>3</sup> The bulk phase structure is optimized first, and the surface models are carried out on this basis to adsorb the Zn atom. Table S2 shows the lattice constants and corresponding k-point mesh of the models. A vacuum of 15 Å was set in order to circumvent periodic interactions between the atoms.

## **2. Supporting Notes**



## **2.1 The strategy for using of TS electrolyte additives and establishment of a dense ZnO@Cu artificial layer on the surface of Zn metal for constructing dendrite-free Zn electrode without side reaction.**

The schematic diagram of the production of Zn anode is shown in Fig. S5a. A simple, low-cost, and environmentally friendly method is used to construct the Zn anode with the required surface modification. First, the Zn foil is annealed in high-temperature air to form a thin ZnO layer on its surface. Then, metallic Cu is deposited on the surface of ZnO to form a double-layer heterogeneous interface by using electrodeposition technology. As mentioned above, Zn electrodes are highly unstable with/without electrolyte additives, and the side reactions will occur during the typical charge/discharge process to form  $\text{Zn}_2\text{SO}_4(\text{OH})_2$ , which decreases the CE, reversible capacity and cycle life of ZIBs. As a comparison, the Zn metal with ZnO@Cu artificial layer not only effectively suppresses the corrosion reaction by preventing the electrolyte, but also induces the  $\text{Zn}^{2+}$  stripping/plating together with the TS electrolyte additive, thereby suppressing the Zn dendrites growth and improving the reversibility of Zn electrode (Fig. S5b). The effect of ZnO@Cu layer on the stability of Zn foil is assessed in 2 M  $\text{ZnSO}_4$  electrolyte, as shown in Figs. S6a and b. After 5 days, the ZnO@Cu/Zn foil still retains a light surface without evident corrosion, which is mainly attributed to the ZnO@Cu protective film isolating to the electrolyte. Similar to Figs. 1d and e, the by-products grow along the Zn metal plane, resulting in a larger size of the deposited Zn plane (Figs. S6c and d), which are further explained in Figs. 2h and 4d. The XRD pattern is gathered after soaking in 2 M  $\text{ZnSO}_4$  electrolyte (Fig.

S7), which is similar to that of ZnO@Cu/Zn foil before immersion and without any peaks for the  $\text{Zn}_2\text{SO}_4(\text{OH})_2$  by-product, demonstrating that the side reactions of the Zn anode with the electrolyte are disrupted.

### 3. Supporting Fig.s

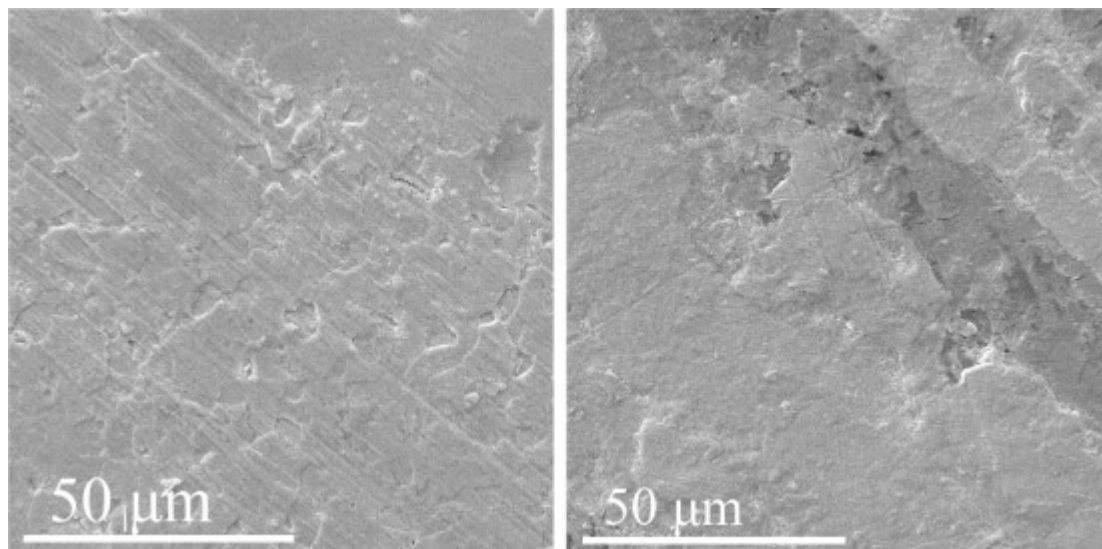


**Fig. S1.** SEM images of bare Zn foil.

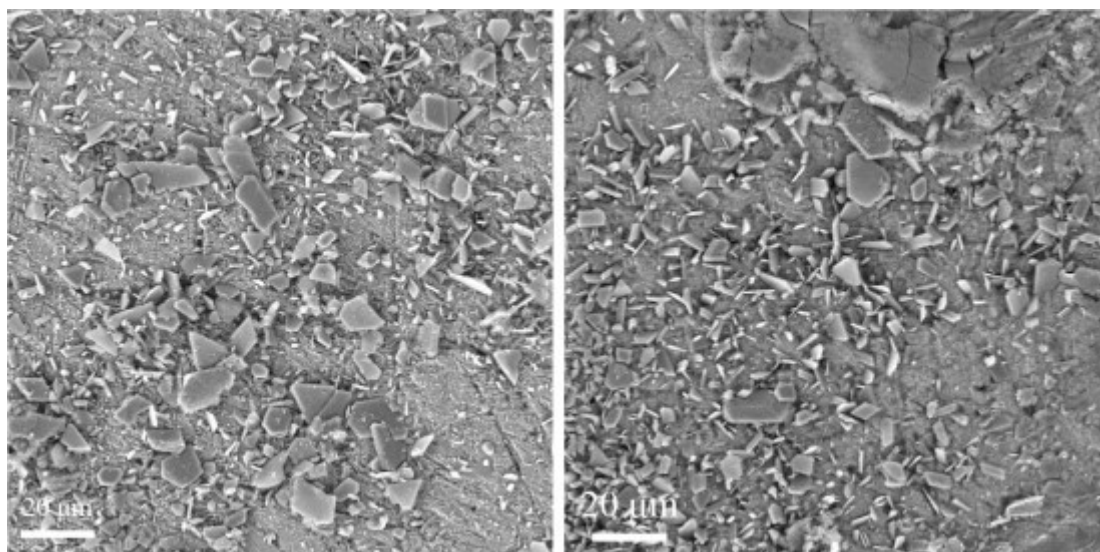


**Fig. S2.** SEM images of the Zn foil in 2 M ZnSO<sub>4</sub> after 5 days.

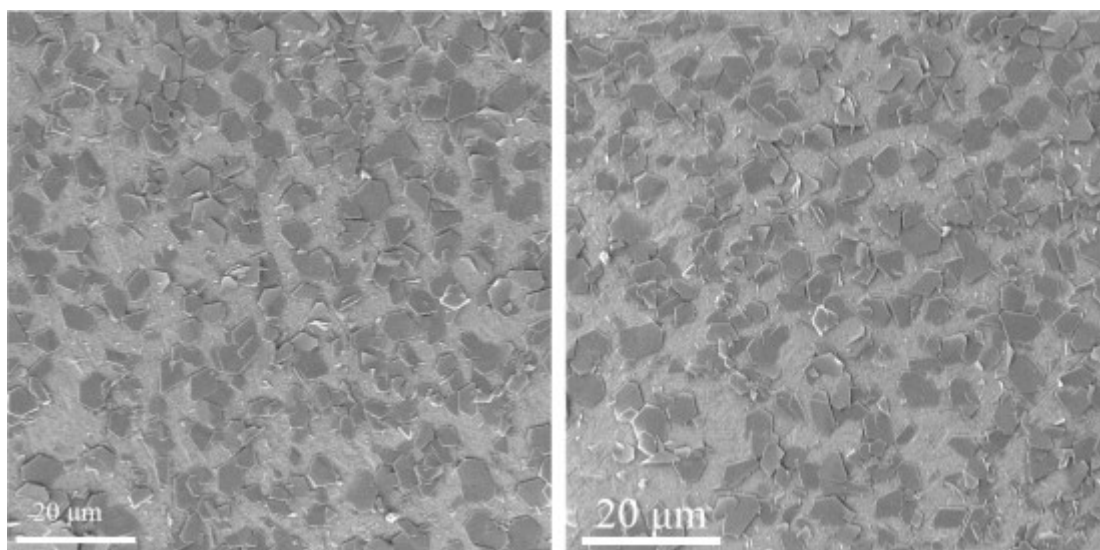


**Fig. S3.** SEM image of Zn foil in 2 M ZnSO<sub>4</sub> with TS after 5 days.

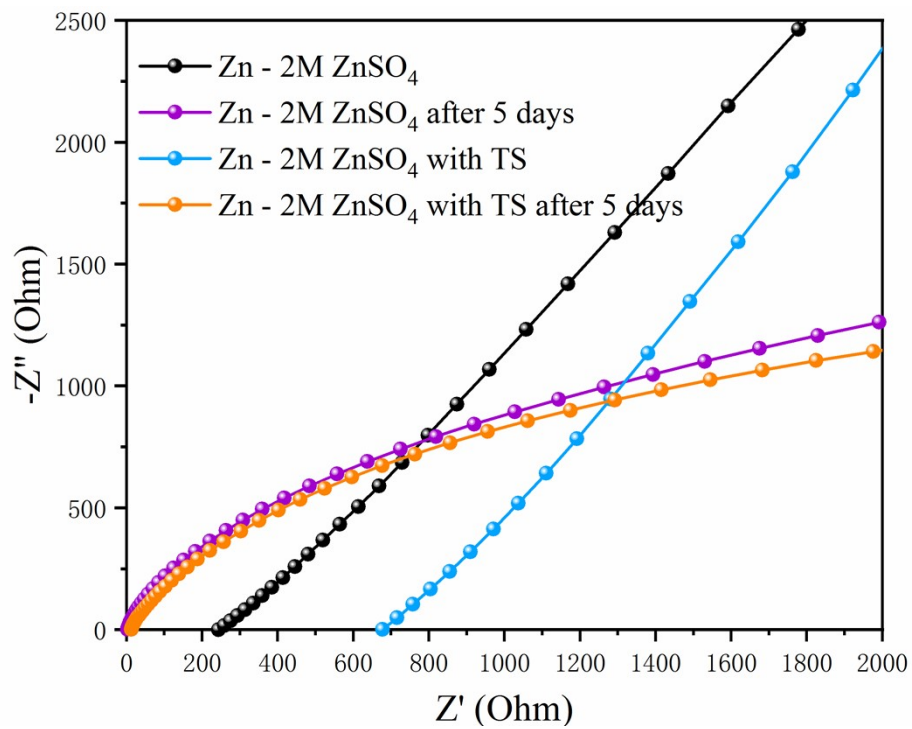


**Fig. S4.** Electrochemical impedance spectroscopy measurements of various Zn cells.

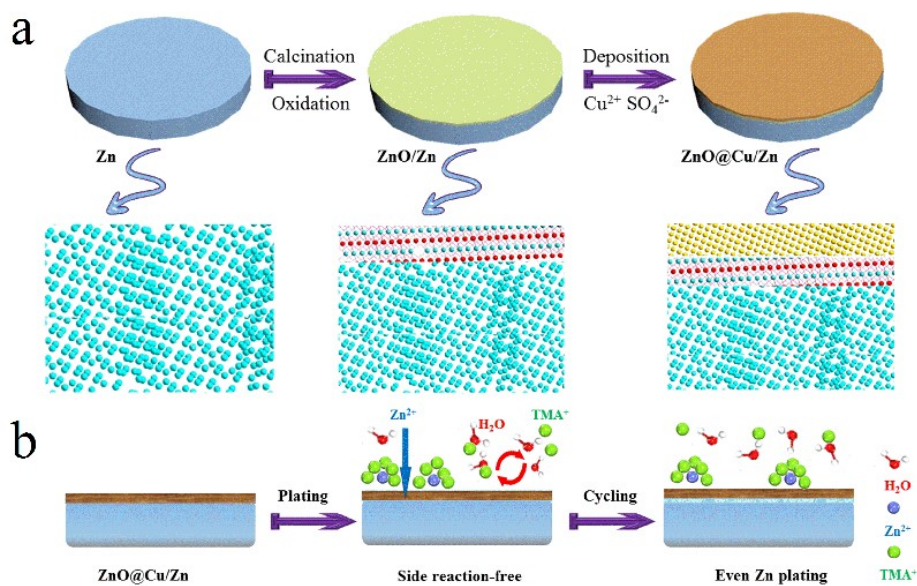


**Fig. S5.** a) Introducing the ZnO@Cu layer on the surface of Zn metal substrate by two-step strategy. b) By incorporating the artificial ZnO@Cu layer on the Zn surface and using TS electrolyte additive, uniform and compact Zn plating behavior without side reactions can be obtained.

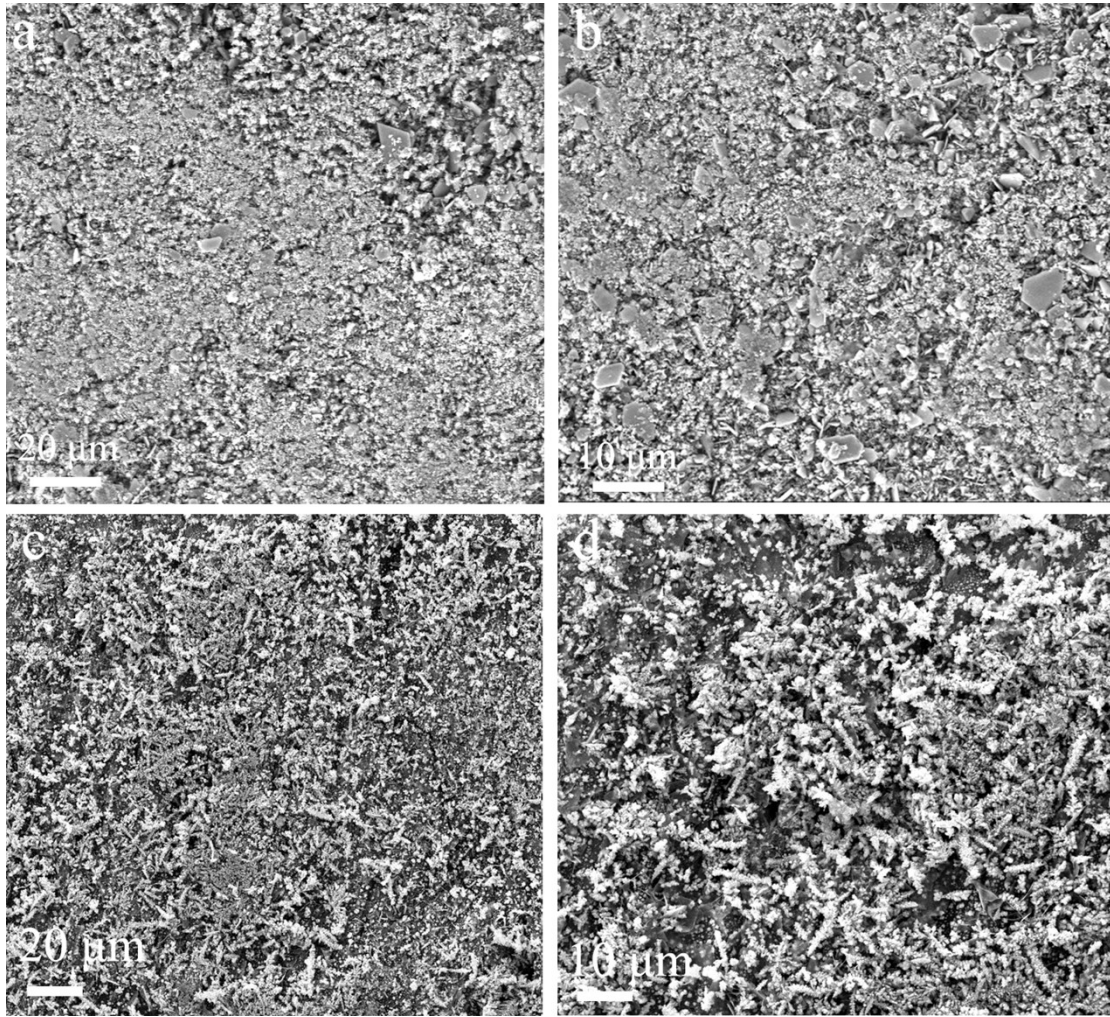


**Fig. S6.** a, b) SEM images of the ZnO@Cu/Zn in pure 2 M ZnSO<sub>4</sub> after 5 days; c, d) SEM images of the ZnO@Cu/Zn in 2 M ZnSO<sub>4</sub> with TS after 5 days.



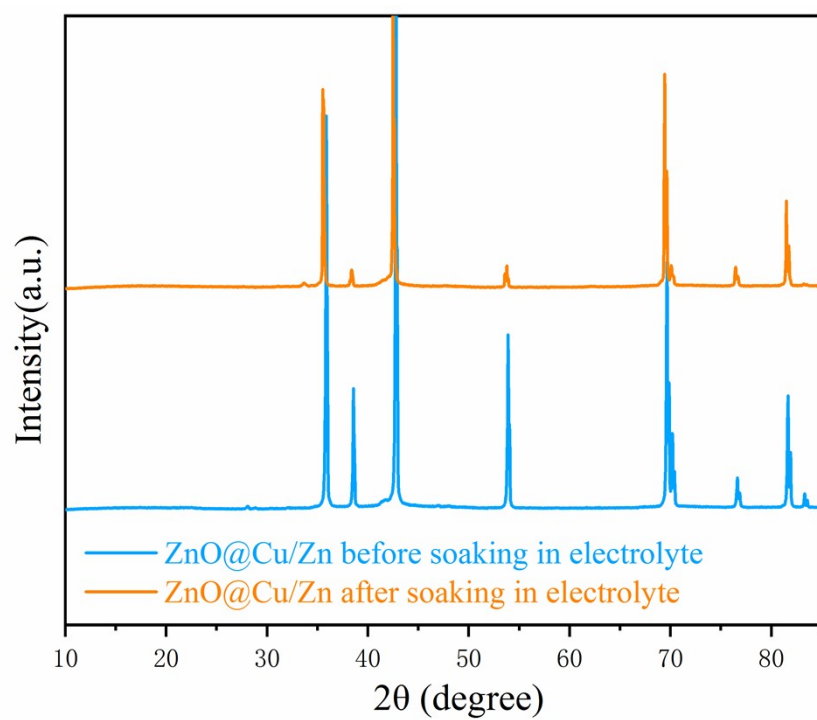


**Fig. S7.** XRD patterns of ZnO@Cu/Zn foil before and after the soaking in 2 M ZnSO<sub>4</sub> for 5 days.

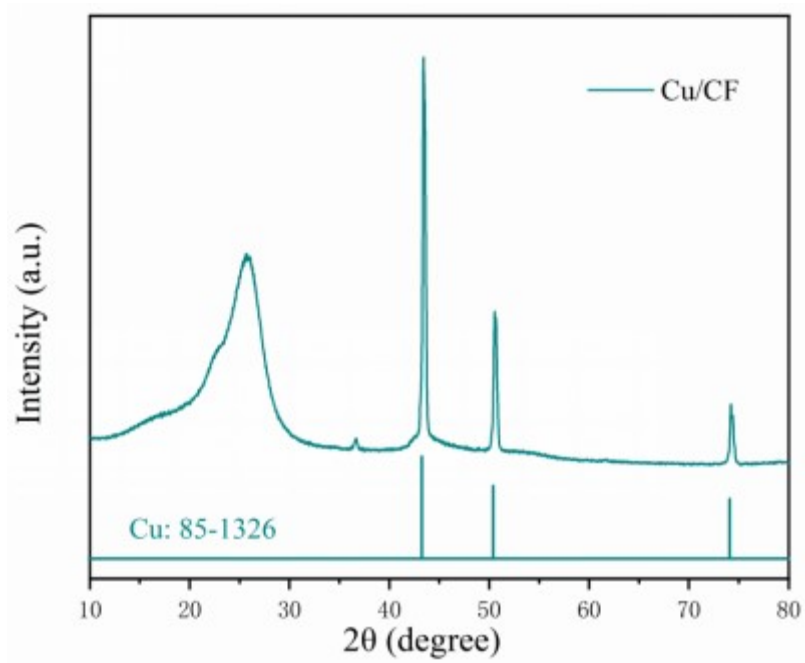


**Fig. S8. f)** X-ray diffraction (XRD) patterns of Cu on Carbon cloth.

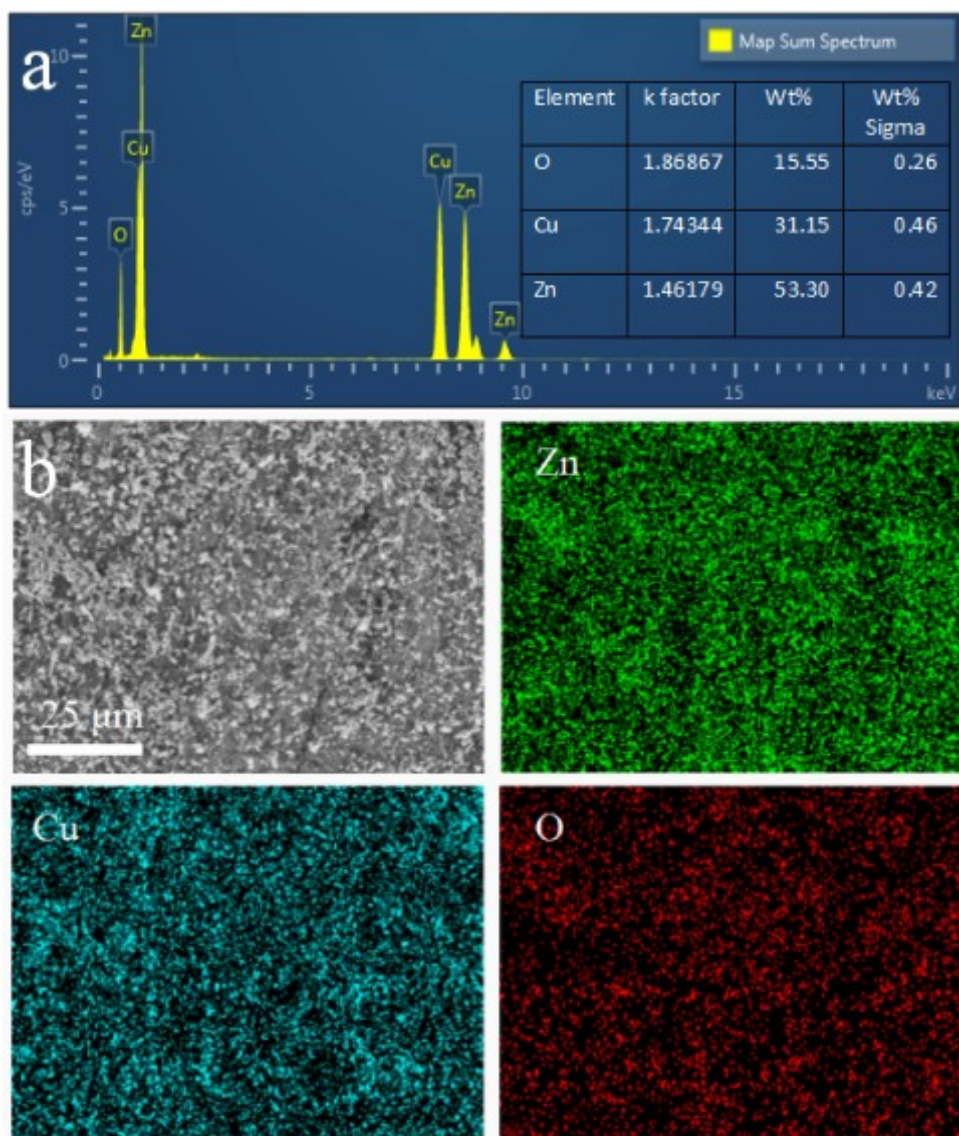


**Fig. S9.** EDS mapping images of ZnO@Cu/Zn including Zn, Cu and O element.

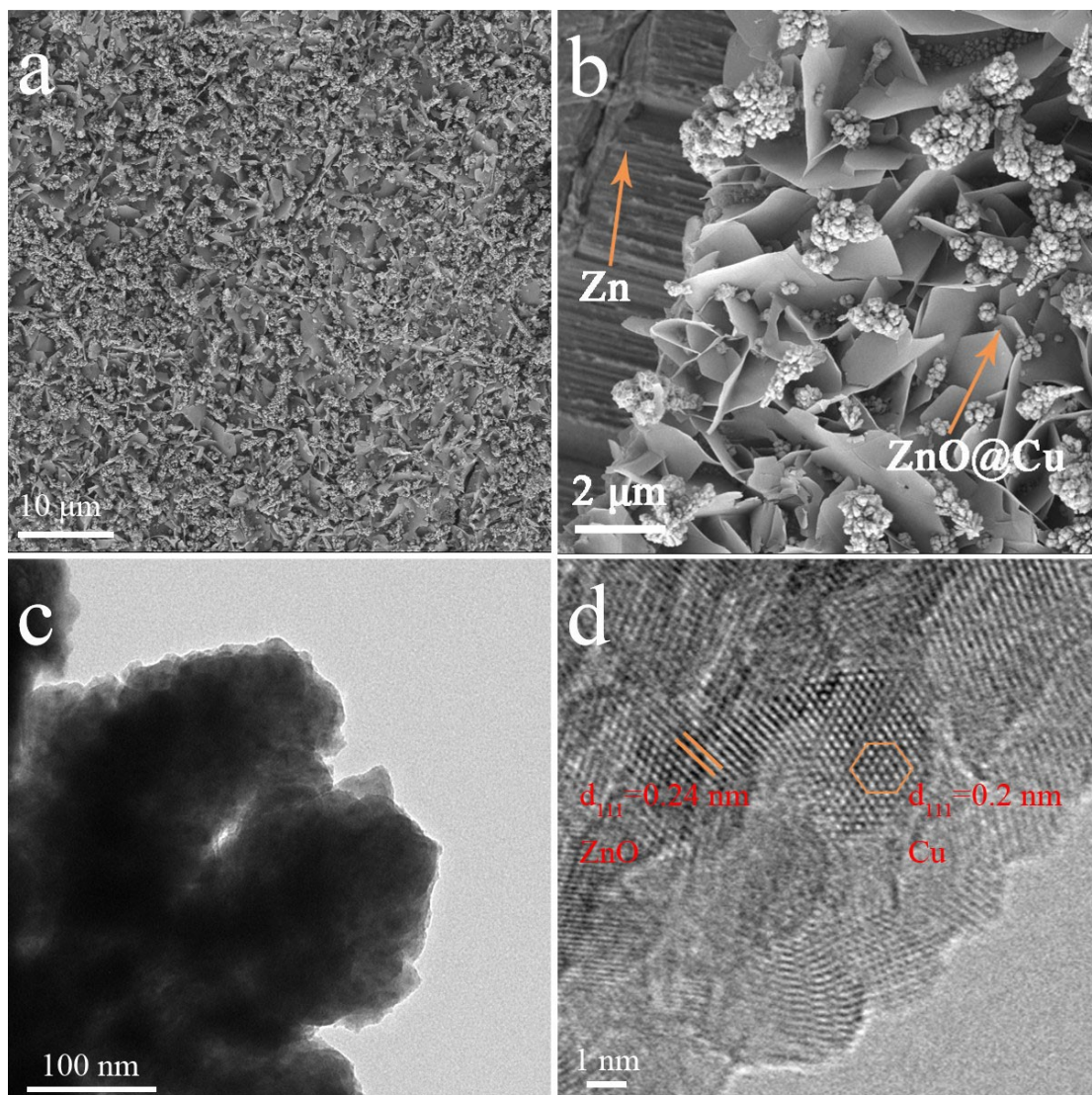


**Fig. S10.** SEM, TEM and HR-TEM images of ZnO@Cu/Zn.



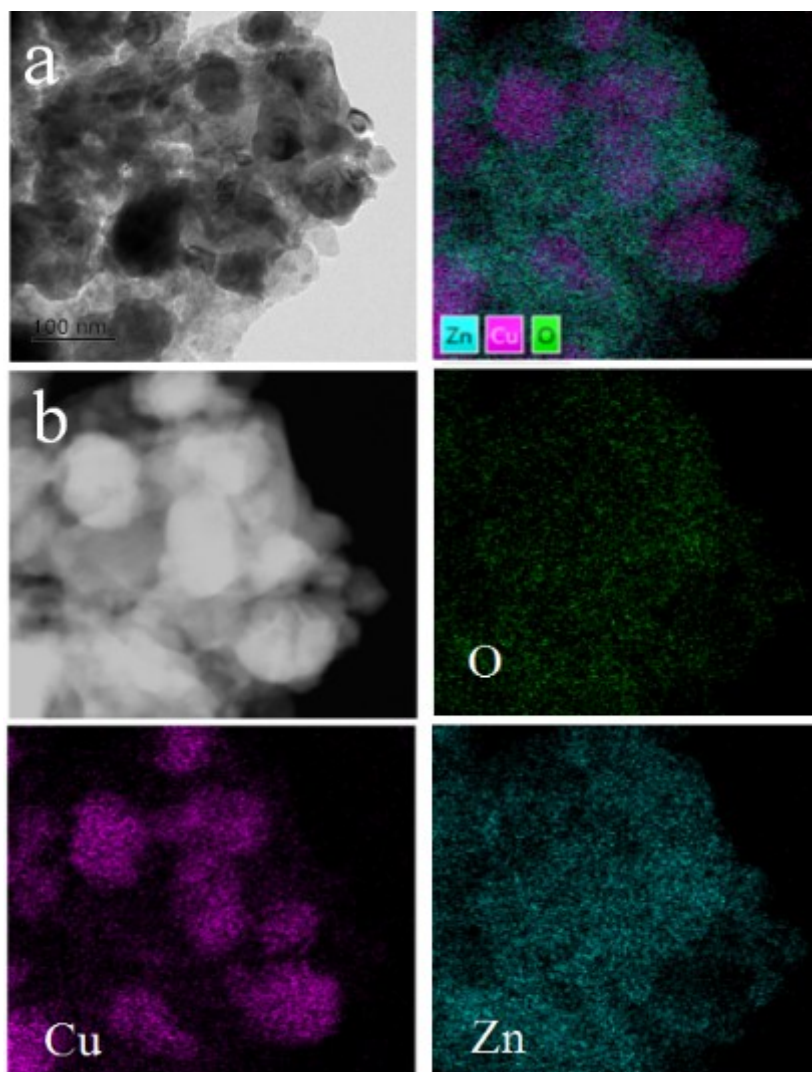


**Fig. S11.** Transmission mapping images of ZnO@Cu/Zn including Zn, Cu and O element.

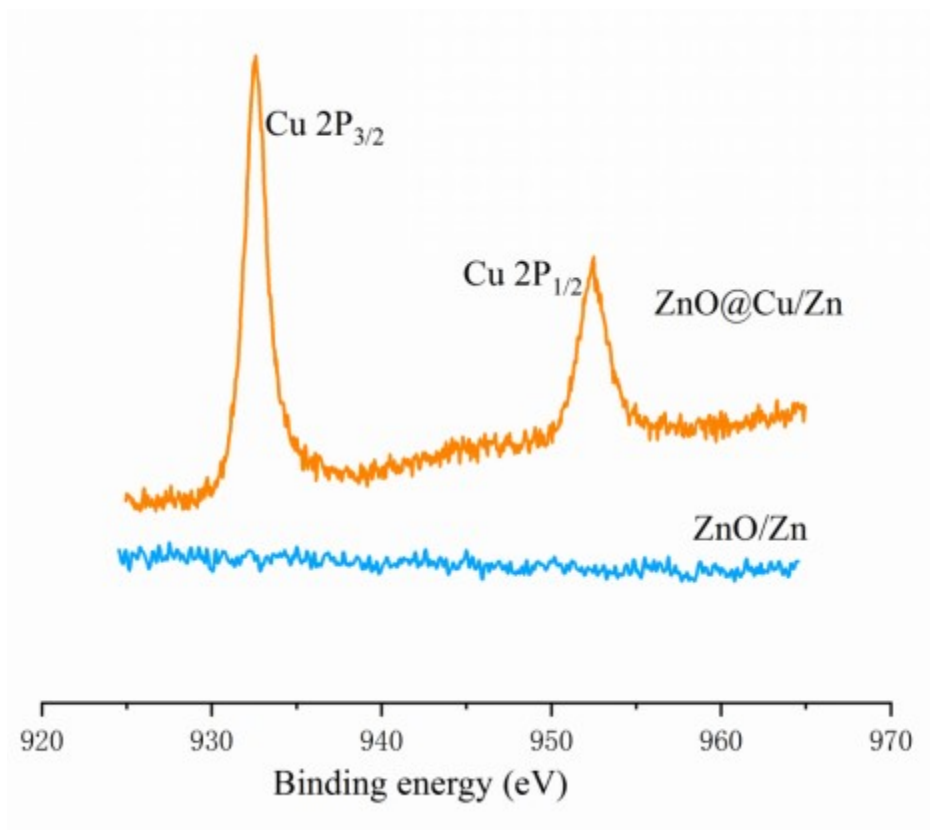


**Fig. S12.** High-resolution XPS spectra of Cu in ZnO/Zn and ZnO@Cu/Zn.

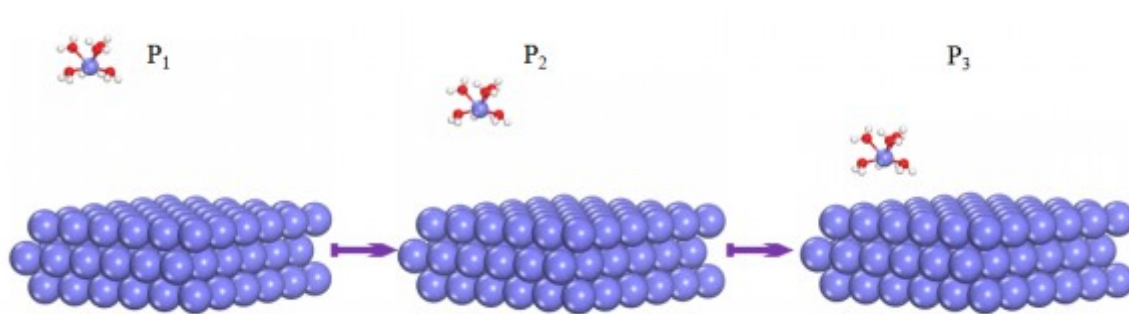


**Fig. S13.** Model of DFT calculations, showing a hydrated Zn<sup>2+</sup> ion passing on a Zn surface.

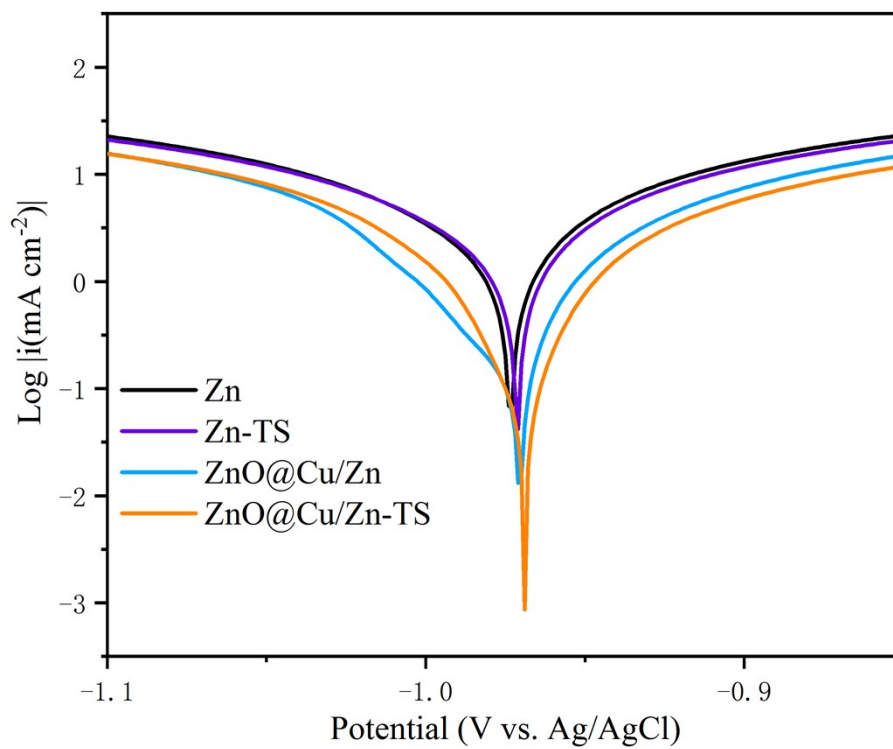


**Fig. S14.** Linear polarization curves showing the corrosion on bare Zn, Zn-TS, ZnO@Cu/Zn and ZnO@Cu/Zn-TS.



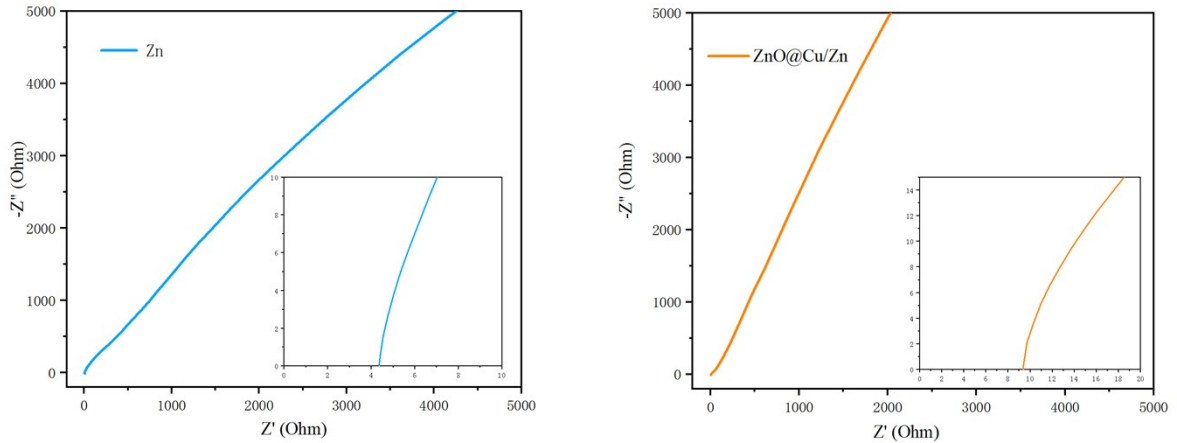


**Fig. S15.** (a) Nyquist plots collected at open circuit voltage (OCV) over the frequency range of 100 kHz to 1 Hz. a) Zn symmetrical cell with glass fibre as separator (inset: enlargement of indicated range). b) ZnO@Cu coated Zn symmetrical cell with glass fibre as separator (inset: enlargement of indicated range).

For the Zn/Zn cell with glass fibre, the ionic conductivity of the glass fibre separator could be calculated from the bulk electrolyte resistance (Fig. S15a) by the following equation:

$$\sigma = \frac{L}{R_b S}$$

where L is the thickness of the glass fibre separator (0.675 mm), S is the contact area (1 cm<sup>2</sup>), and R<sub>b</sub> (glass fibre) = ~4.4 ohm at room temperature. Thus,  $\sigma_{\text{glass fibre}} = 1.53 \times 10^{-2} \text{ S cm}^{-1}$ . For the ZnO@Cu coated Zn symmetrical cell, R<sub>b</sub> (ZnO@Cu) = R<sub>b</sub> – R<sub>b</sub> (glass fibre) = 9.4 ohm (Fig. S15b). Therefore, the ionic conductivity of the ZnO@Cu film can be evaluated as  $\sigma_{\text{ZnO@Cu}} = \sim 1.9 \times 10^{-4} \text{ S}\cdot\text{cm}^{-1}$ .

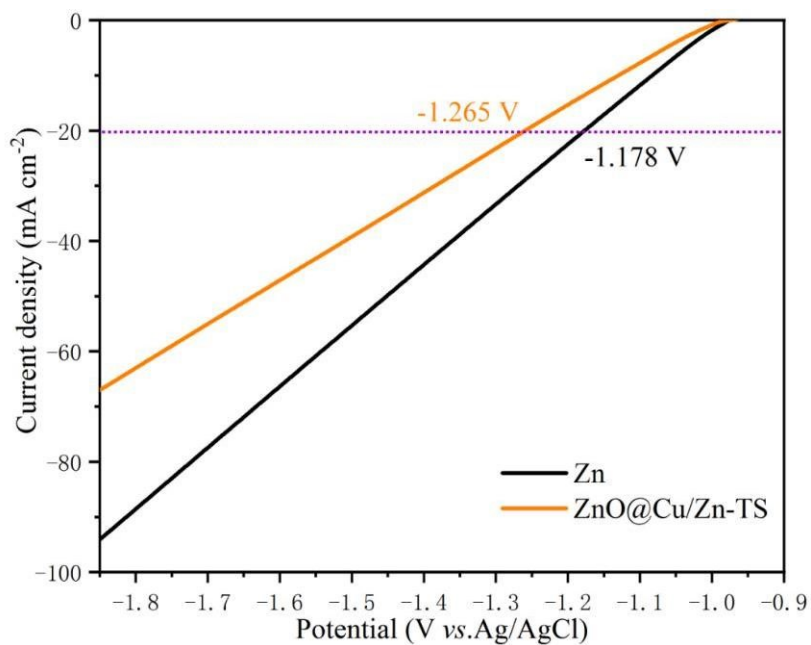


**Fig. S16.** Comparison of HER performance under Zn and ZnO@Cu/Zn-TS electrodes systems.

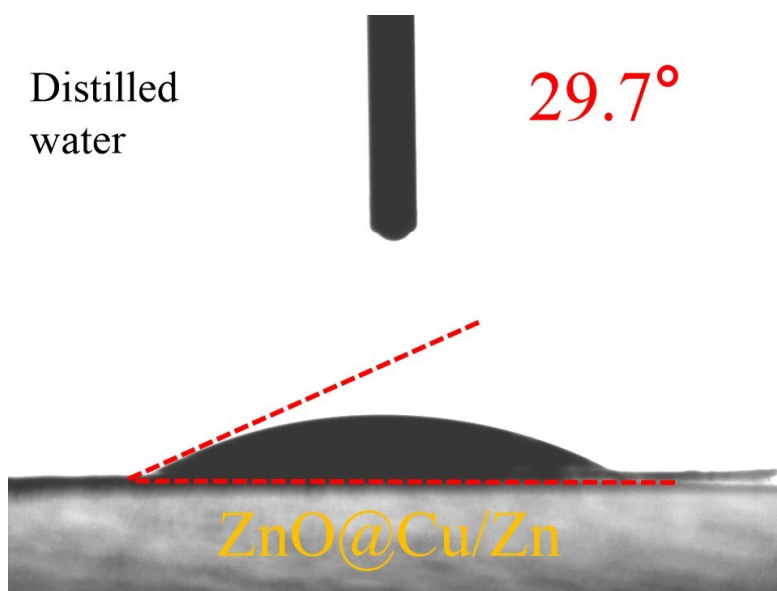


**Fig. S17.** The contact angle measurement results for the fabricated ZnO@Cu/Zn anodes using distilled water.

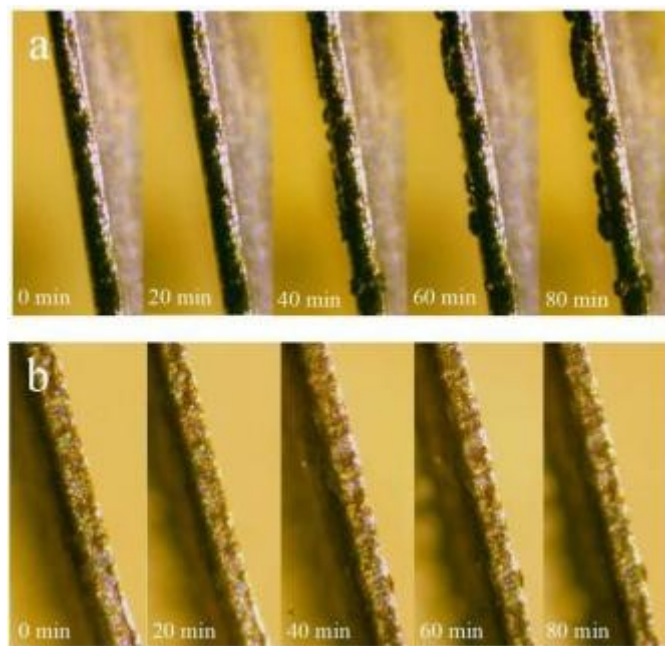


**Fig. S18.** a) Zn-TS and b) ZnO@Cu/Zn electrodes in symmetric transparent cells, along with the specified numbers of plating/stripping cycles.

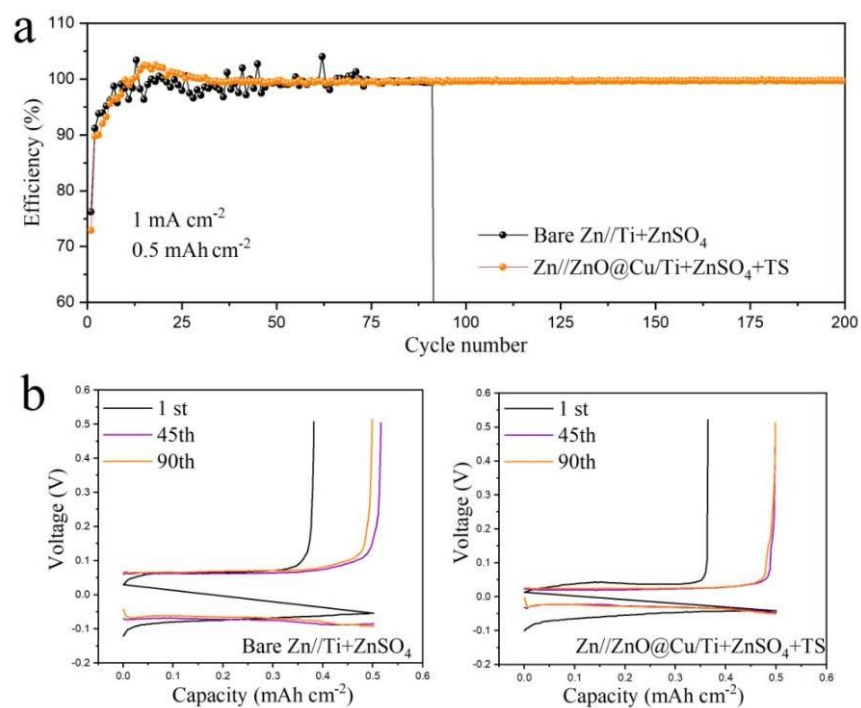


**Fig. S19.** Coulombic efficiency (CE) measurements of Zn//Ti and Zn//ZnO@Cu/Ti-TS cells under different electrolyte system and b) corresponding voltage profiles at various cycles.

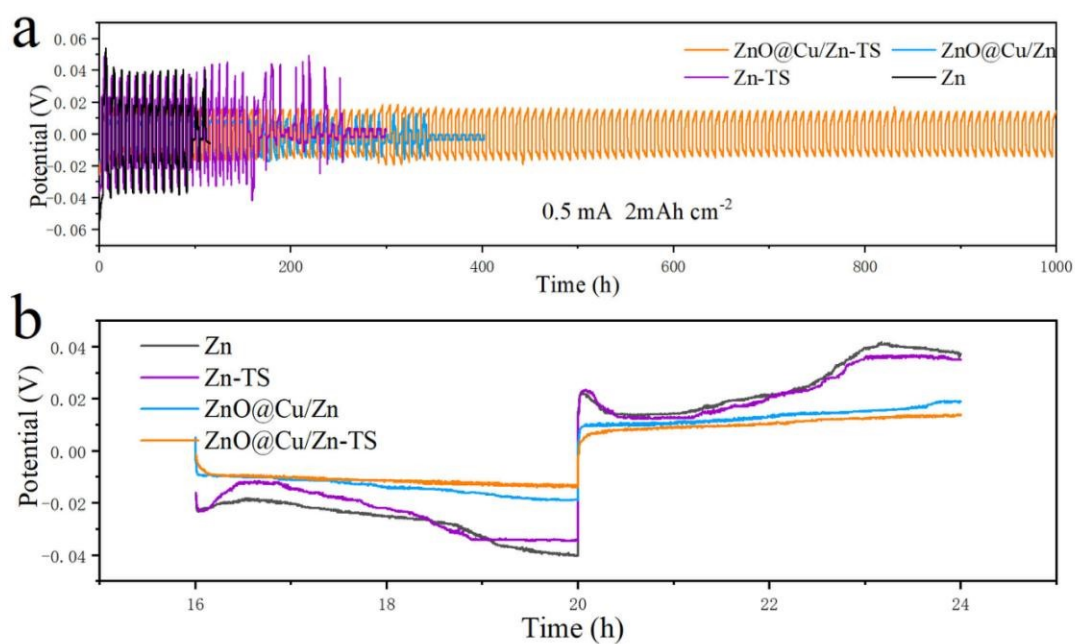


**Fig. S20.** a) Comparison of the cycling stability of Zn, Zn-TS, ZnO@Cu/Zn and ZnO@Cu/Zn-TS symmetric cell at 0.5 mA cm<sup>-2</sup> with the capacity of 2 mA h cm<sup>-2</sup>; b) High-resolution voltage profiles at 0.5 mA cm<sup>-2</sup> with the capacity of 2 mA h cm<sup>-2</sup> for the first cycle.

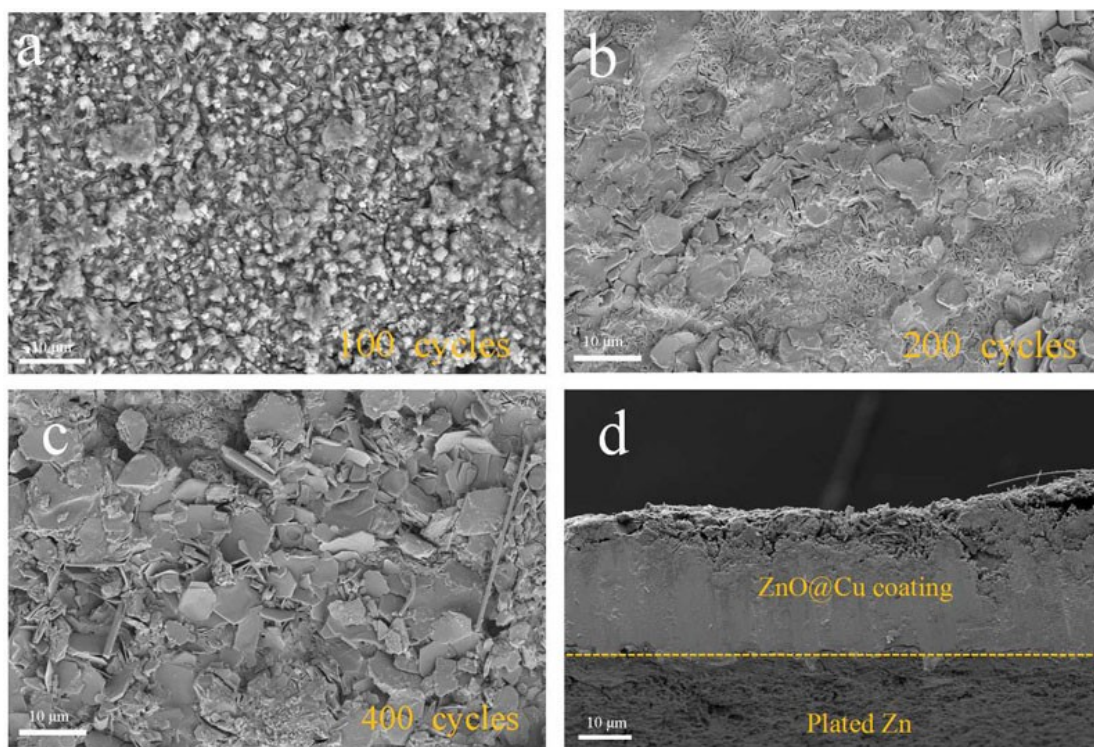


**Fig. S21.** Top-view SEM images of Zn deposition for ZnO@Cu/Zn-TS electrodes after a) 100 cycles, b) 200 cycles and c) 400 cycles; d) Cross-sectional SEM image of Zn deposition for ZnO@Cu/Zn-TS electrodes after 400 cycles at  $10 \text{ mA cm}^{-2}$  and  $2 \text{ mAh cm}^{-2}$ .

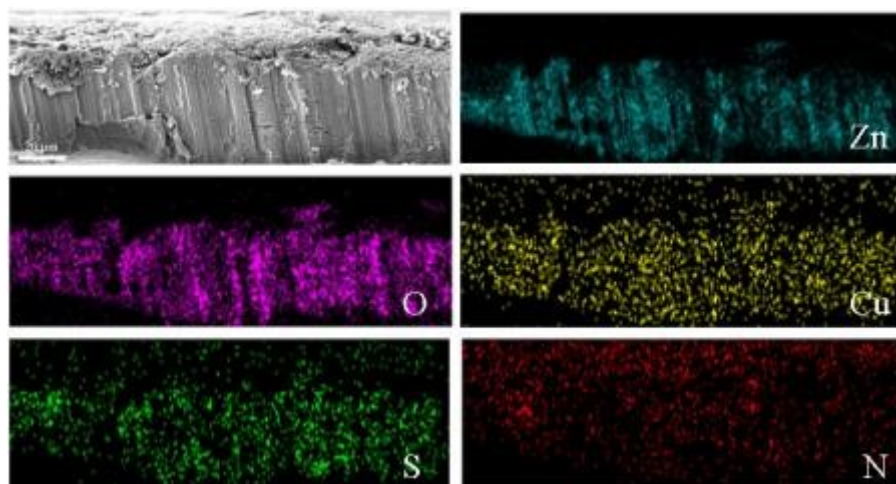


**Fig. S22.** Cross-sectional mapping images of ZnO@Cu/Zn including Zn, Cu and O element of Zn deposition for ZnO@Cu/Zn-TS electrodes after 400 cycles at  $10 \text{ mA cm}^{-2}$  and  $2 \text{ mAh cm}^{-2}$ .

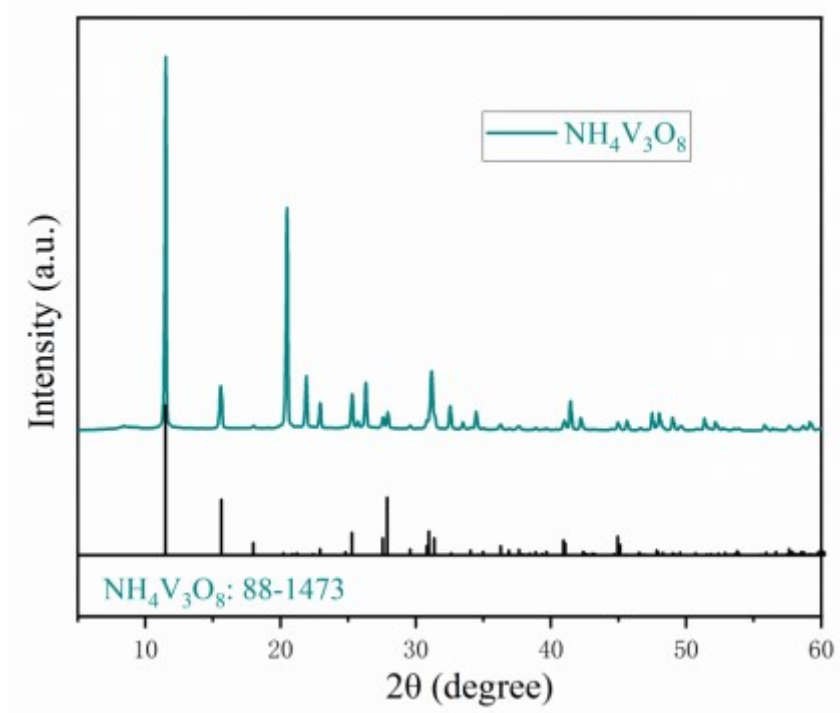


**Fig. S23.** XRD pattern of  $\text{NH}_4\text{V}_3\text{O}_8$ .



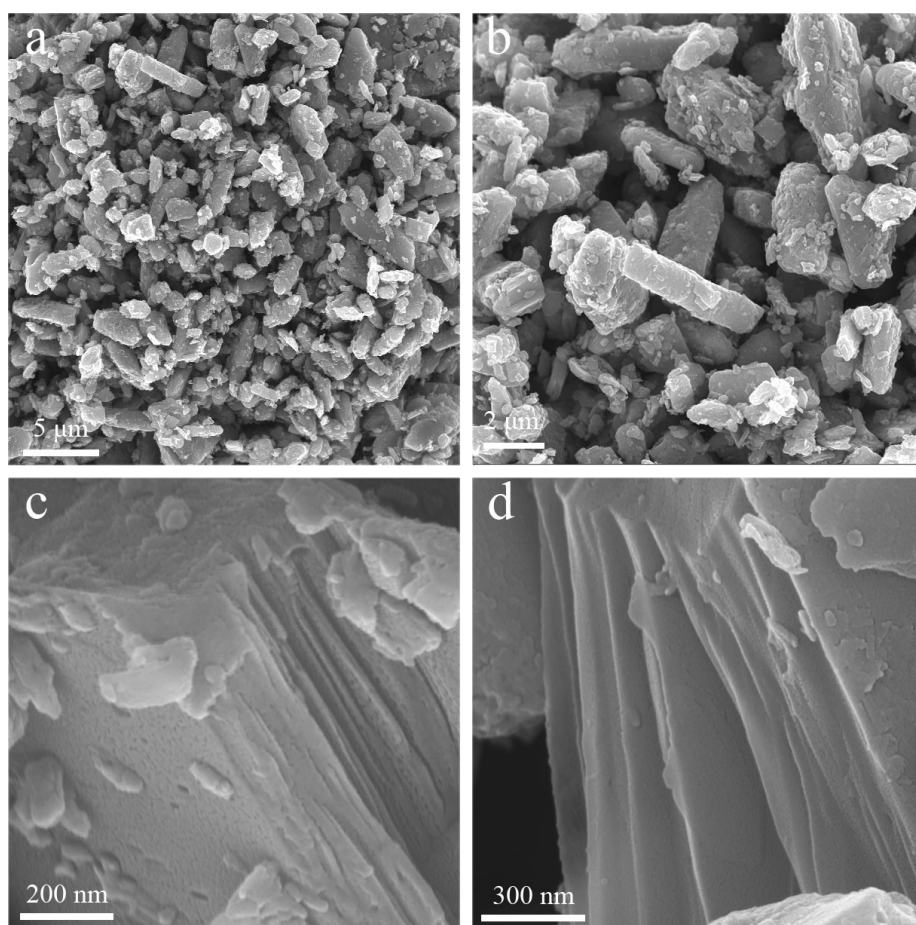


**Fig. S24.** SEM images of  $\text{NH}_4\text{V}_3\text{O}_8$ .

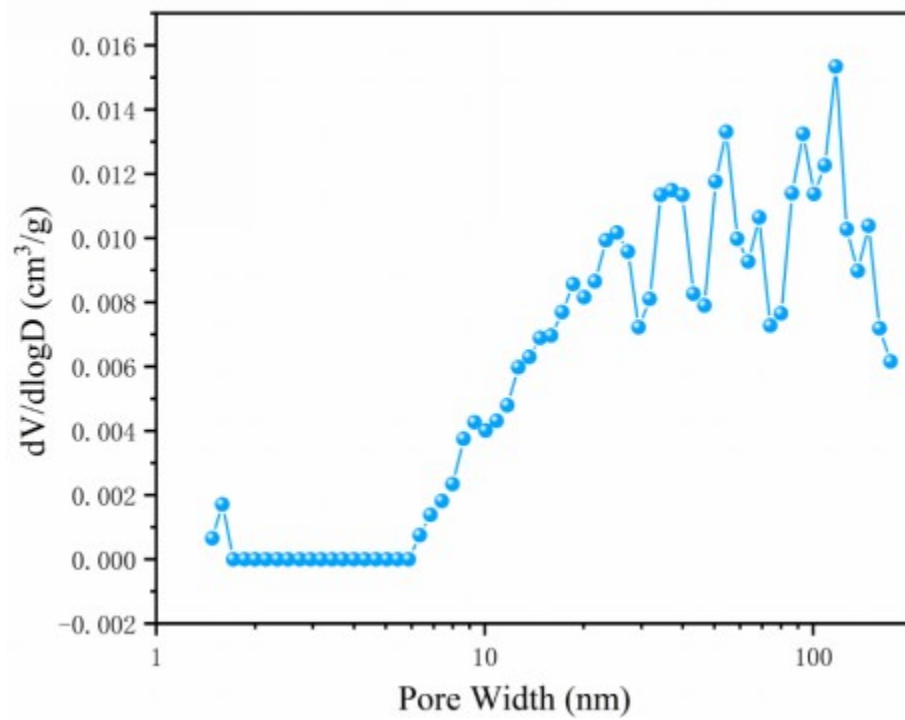


**Fig. S25.** Pore size distribution curves of  $\text{NH}_4\text{V}_3\text{O}_8$ .

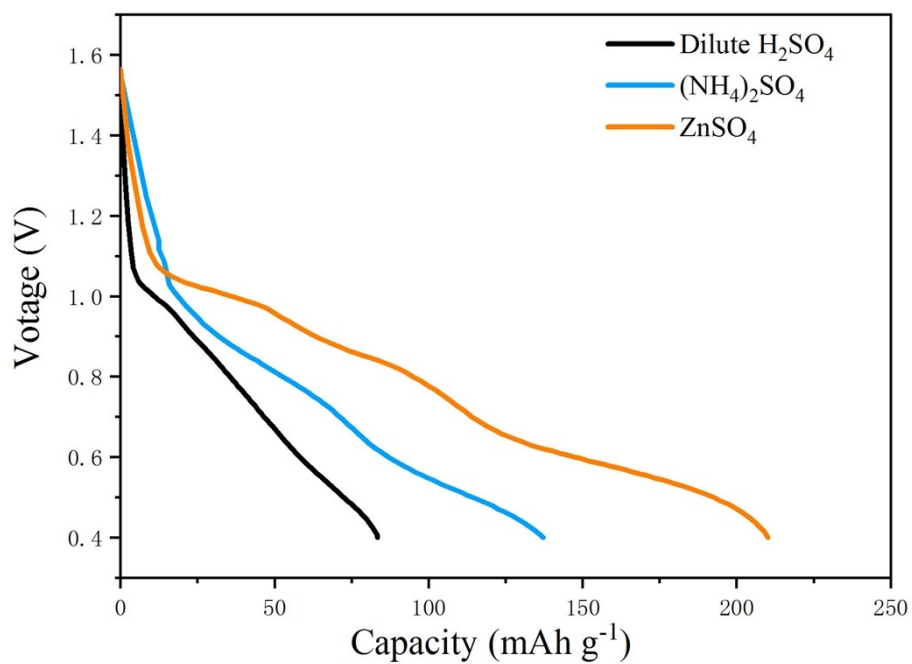


**Fig. S26.** Typical charge-discharge curves of  $\text{NH}_4\text{V}_3\text{O}_8|\text{Zn}$  batteries with dilute  $\text{H}_2\text{SO}_4$  (PH value:5), 0.5 M  $(\text{NH}_4)_2\text{SO}_4$  and 2 M  $\text{ZnSO}_4$  electrolytes at the current density of  $0.2 \text{ A g}^{-1}$ .

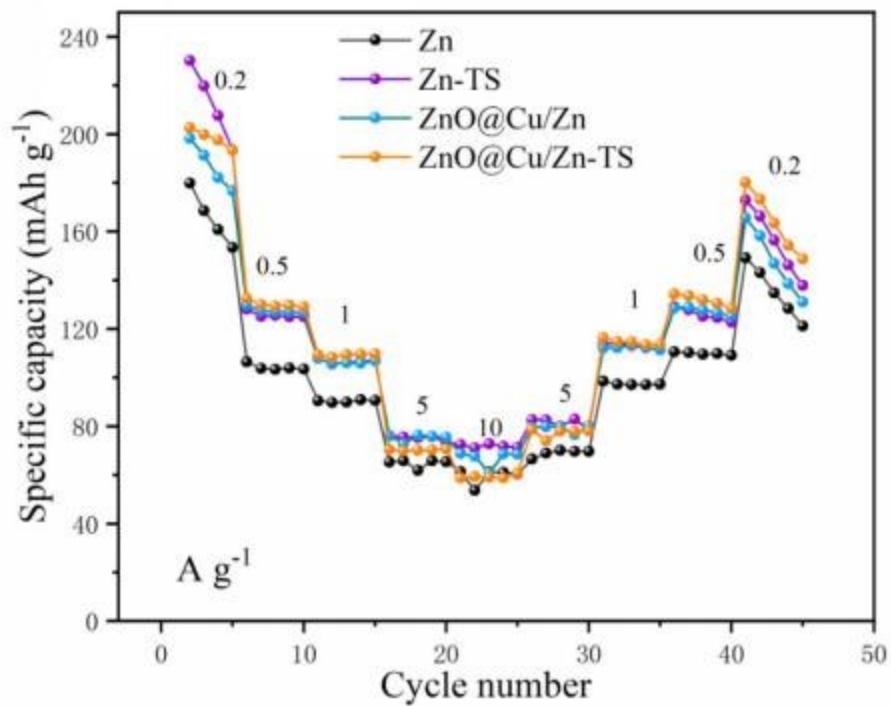


**Fig. S27.** Rate performance based on charging/discharging curves of the  $\text{NH}_4\text{V}_3\text{O}_8/\text{Zn}$ ,  $\text{NH}_4\text{V}_3\text{O}_8/\text{Zn-TS}$ ,  $\text{NH}_4\text{V}_3\text{O}_8/\text{ZnO@Cu/Zn}$  and  $\text{NH}_4\text{V}_3\text{O}_8/\text{ZnO@Cu/Zn-TS}$  battery.

**Table S1.** Comparison of the adsorption energy of  $Zn^{2+}$  ions of Zn, ZnO and Cu at bridge, top and hole view.

Zn (111)	Cu (111)		ZnO(001)		
Bridge (eV)	-0.484	Bridge	-1.368	O-hole	-4.640
Top (eV)	-0.630	Top	-1.113	Zn-hole	-4.677
Hole (eV)	-0.498	Hole	-1.405		

**Table S2.** The calculated lattice constants and corresponding k-point mesh of the bulk and surface structures.

	a /Å	b /Å	c /Å	$\alpha /^\circ$	$\beta /^\circ$	$\gamma /^\circ$	k-point
Zn	2.566	2.566	5.035	90.00	90.00	90.00	$11 \times 11$ $\times 5$
Cu	3.545	3.545	3.545	90.00	90.00	90.00	$7 \times 7 \times 7$
ZnO	4.238	4.238	4.238	90.00	90.00	90.00	$6 \times 6 \times 6$
Zn(001)	5.133	5.133	/	90.00	90.00	120.00	$6 \times 6 \times 1$
Cu(111)	5.014	5.014	/	90.00	90.00	120.00	$6 \times 6 \times 1$
ZnO(111)	5.190	5.190	/	90.00	90.00	120.00	$6 \times 6 \times 1$

**Table S3.** Results of electrical conductivity measurement performed on Zn foil, ZnO@Cu/Zn and

ZnO@Cu powder.

Electrode Materials	Resistivity ( $\Omega\cdot\text{cm}$ )
Zn foil	0.0626
ZnO@Cu/Zn	0.0715
ZnO@Cu powder	16.54

**Table S4.** Comparison of the electrolyte additives or artificial layer of symmetric cells for Zn

dendrite inhibition.

Artificial layer/additives (ZnSO <sub>4</sub> solution)	Current density with capacity	cycle life	Ref.
Zif-67 layer	2 mA cm <sup>-2</sup> with 1 mAh cm <sup>-2</sup>	1200 h	[4] <i>Adv. Sci.</i> <b>2020</b> , 2002173
polyvinyl butyral layer	0.5 mA cm <sup>-2</sup> with 0.5 mAh cm <sup>-2</sup>	2200 h	[5] <i>Adv. Funct. Mater.</i> <b>2020</b> , 2001263
polyacrylamide electrolyte additive	1 mA cm <sup>-2</sup> with 1 mAh cm <sup>-2</sup>	280 h	[6] <i>Angew. Chem, Int. Ed.</i> <b>2019</b> , 58, 15841–15847

3D-ZnO layer	5 mA cm <sup>-2</sup> with 1.25 mAh cm <sup>-2</sup>	500 h	[7] <i>Energy Environ. Sci.</i> <b>2020</b> , <i>13</i> , 503-510
Anhydrous Acetonitrile electrolyte additive	1 mA cm <sup>-2</sup> with 1 mAh cm <sup>-2</sup>	1,300 h	[8] <i>Electrochimica Acta.</i> <b>2020</b> , <i>358</i> , 136937
ethylene glycol electrolyte additive	5 mA cm <sup>-2</sup> with 0.5 mAh cm <sup>-2</sup>	800 h	[9] <i>Nano Energy.</i> <b>2021</b> , <i>80</i> , 105478
tetrabutylammonium sulfate electrolyte additive	5 mA cm <sup>-2</sup> with 2 mAh cm <sup>-2</sup>	500 h	[10] <i>ACS Energy Lett.</i> <b>2020</b> , <i>5</i> , 3012–3020
NaTi <sub>2</sub> (PO <sub>4</sub> ) <sub>3</sub> layer	1 mA cm <sup>-2</sup> with 1 mAh cm <sup>-2</sup>	260 h	[11] <i>Adv. Funct. Mater.</i> <b>2020</b> , <i>30</i> , 2004885
ZnS layer	2 mA cm <sup>-2</sup> with 2 mAh cm <sup>-2</sup>	1,100 h	[12] <i>Adv. Mater.</i> <b>2020</b> , 2003021
Glucose electrolyte additive	1 mA cm <sup>-2</sup> with 1 mAh cm <sup>-2</sup>	2,000 h	[13] <i>Angew. Chem. Int. Ed.</i> <b>2021</b> , <i>60</i> , 2–1
ZrO <sub>2</sub> layer	0.25 mA cm <sup>-2</sup> with 0.125 mAh cm <sup>-2</sup>	3,800 h	[14] <i>Adv. Funct. Mater.</i> <b>2020</b> , <i>30</i> , 1908528
ZnO@Cu layer and TS additive	10 mA cm <sup>-2</sup> with 2 mAh cm <sup>-2</sup>	over 1000h	Present work
ZnO@Cu layer and TS additive	0.5 mA cm <sup>-2</sup> with 2 mAh cm <sup>-2</sup>	over 1000h	Present work
ZnO@Cu layer and TS additive	0.25 mA cm <sup>-2</sup> with 0.125 mAh cm <sup>-2</sup>	over 4,500 h	Present work

## References:

- [1] G. Kresse, J. Hafner, *Phys Rev B Condens Matter*, *1993*, **47**, 558-561.
- [2] J. P. Perdew, K. Burke, Ernzerhof M, *Phys Rev Lett*, *1996*, **77**, 3865-3868.

- [3] S. Grimme, J. Antony, S. Ehrlich, H. Krieg, *J Chem Phys*, 2010, **132**, 154104.
- [4] X. Liu, F. Yang, W. Xu, Y. Zeng, J. He, X. Lu, *Adv. Sci*, 2020, **7**, 2002173.
- [5] J. Hao, X. Li, S. Zhang, F. Yang, X. Zeng, S. Zhang, G. Bo, C. Wang, Z. Guo, *Adv. Funct. Mater*, 2020, **30**, 2001263.
- [6] Q. Zhang, J. Luan, L. Fu, S. Wu, Y. Tang, X. Ji, H. Wang, *Angew. Chem, Int. Ed*, 2019, **58**, 15841-15847.
- [7] X. Xie, S. Liang, J. Gao, S. Guo, J. Guo, C. Wang, G. Xu, X. Wu, G. Chen, J. Zhou, *Energy Environ. Sci*, 2020, **13**, 503-510.
- [8] J. Shi, K. Xia, L. Liu, C. Liu, Q. Zhang, L. Li, X. Zhou, J. Liang, Z. Tao, *Electrochimica Acta*, 2020, **358**, 136937.
- [9] R. Qin, Y. Wang, M. Zhang, Y. Wang, S. Ding, A. Song, H. Yi, L. Yang, Y. Song, Y. Cui, J. Liu, Z. Wang, S. Li, Q. Zhao, F. Pan, *Nano Energy*, 2021, **80**, 105478.
- [10] A. Bayaguud, X. Luo, Y. Fu, C. Zhu, *ACS Energy Lett*, 2020, **5**, 3012-3020.
- [11] M. Liu, J. Cai, H. Ao, Z. Hou, Y. Zhu, Y. Qian, *Adv. Funct. Mater*, 2020, **30**, 2004885.
- [12] J. Hao, B. Li, X. Li, X. Zeng, S. Zhang, F. Yang, S. Liu, D. Li, C. Wu, Z. Guo, *Adv. Mater*, 2020, **32**, 2003021.
- [13] P. Sun, L. Ma, W. Zhou, M. Qiu, Z. Wang, D. Chao, W. Mai, *Angew. Chem. Int. Ed*, 2021, **60**, 2-1.
- [14] P. Liang, J. Yi, X. Liu, K. Wu, Z. Wang, J. Cui, Y. Liu, Y. Wang, Y. Xia, Ji. Zhang, *Adv. Funct. Mater*, 2020, **30**, 1908528.



